Mathematical and numerical model to study two-dimensional free flow isoelectric focusing

Kisoo Yoo,[1,a)] Jaesool Shim,[2,a)] Jin Liu,[1] and Prashanta Dutta[1,b)]
[1]*School of Mechanical and Materials Engineering, Washington State University, Pullman, Washington 99164-2920, USA*
[2]*School of Mechanical Engineering, Yeungnam University, Gyeongsan, Gyeonsanbukdo, South Korea*

(Received 27 April 2014; accepted 4 June 2014; published online 11 June 2014)

Even though isoelectric focusing (IEF) is a very useful technique for sample concentration and separation, it is challenging to extract separated samples for further processing. Moreover, the continuous sample concentration and separation are not possible in the conventional IEF. To overcome these challenges, free flow IEF (FFIEF) is introduced in which a flow field is applied in the direction perpendicular to the applied electric field. In this study, a mathematical model is developed for FFIEF to understand the roles of flow and electric fields for efficient design of microfluidic chip for continuous separation of proteins from an initial well mixed solution. A finite volume based numerical scheme is implemented to simulate two dimensional FFIEF in a microfluidic chip. Simulation results indicate that a pH gradient forms as samples flow downstream and this pH profile agrees well with experimental results validating our model. In addition, our simulation results predict the experimental behavior of p*I* markers in a FFIEF microchip. This numerical model is used to predict the separation behavior of two proteins (serum albumin and cardiac troponin I) in a two-dimensional straight microchip. The effect of electric field is investigated for continuous separation of proteins. Moreover, a new channel design is presented to increase the separation resolution by introducing cross-stream flow velocity. Numerical results indicate that the separation resolution can be improved by three folds in this new design compare to the conventional straight channel design. © *2014 AIP Publishing LLC*. [http://dx.doi.org/10.1063/1.4883575]

I. INTRODUCTION

Free flow electrophoresis (FFE) is a widely used analytical technique in proteomics for continuous and simultaneous fractionation and separation of samples.[1,2] In FFE, a thin sheath of laminar flow is introduced perpendicular to the direction of the applied electric field (Figure 1), which affects the position of charged particles or solutes. Since the separated samples flow with the fluid field, this technique is capable of separating and collecting analytes continuously. This continuous separation characteristic makes this technique suitable for preparative applications. The primary advantages of FFE are that the separated samples can be easily extracted and enzymatic activity of the separands can be preserved.[3]

In FFE, a number of separation methods can be used depending on the applications. This includes zone electrophoresis, isotachophoresis, field step electrophoresis, and isoelectric focusing.[2] Among them, isoelectric focusing is very promising as this technique can be used for high resolution separation of proteins, peptides and bacteria. In isoelectric focusing analytes are separated at their isoelectric points (p*I*s) in a pH field by applying an external electric field.

[a)]K. Yoo and J. Shim contributed equally to this work.
[b)]Author to whom correspondence should be addressed. Electronic mail: dutta@mail.wsu.edu. Tel.: (509)335-7989. Fax: (509) 335-4662.

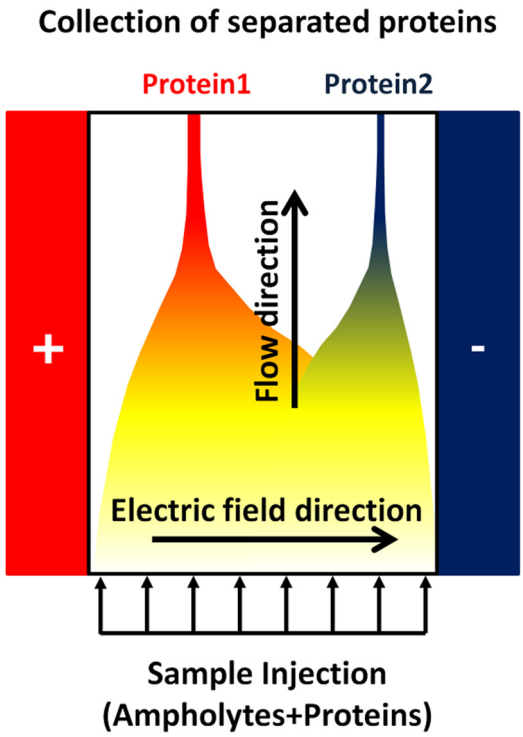

FIG. 1. Schematic of FFIEF system. A flow field is applied perpendicular to the applied electric field. Separation and concentration of analytes take place as they move downstream with buffer flow. Separated and concentrated samples can be collected at the channel outlet.

Generally, the carrier ampholytes (low molecular weight amphoteric molecules) are used to form the pH gradient in the system. The carrier ampholytes are loaded in the separation device during or before introducing the samples. Once an electric field is applied, the carrier ampholytes first form a pH gradient, which helps the analytes to be separated at their respective p*I*s.

In recent years, there is a growing interest in developing miniature device for performing free flow electrophoresis in conjunction with isoelectric focusing as these low cost miniaturized devices can perform the separation in a couple of minutes. Also, because of the ultra small length scales (typically 1–100 μm), these microdevices minimize the sample degradation from Joule heating by dissipating heat quickly. The microscale free flow isoelectric focusing (FFIEF) is first demonstrated by Cabreara and Yager.[4] They have shown the possibility of purifying samples by separating bacteria in a very simple microfluidic device.[4] However, even though their work has demonstrated the feasibility of FFIEF in a microchip, it was severely restricted to low applied electric fields because of bubble formation at the electrode surfaces. To circumvent the bubble problem, Kohlheyer *et al.*[5,6] introduced a modified FFIEF micro-device by adopting anodic and cathodic sheath flows. In their experimental work, a linear pH gradient was developed and the separation of p*I* makers was accomplished. Lately, Wen *et al.*[7,8] utilized an ion permeable poly gel membrane instead of sheath flow and presented a method to improve the separation resolution. Their study reveals that the flow pattern, channel dimension, and IEF conditions highly affect the separation resolution. Therefore, to develop a highly efficient FFIEF microdevice, it is important to determine the design parameters such as channel dimension, applied electric potential, and applied flow velocity of the buffer solution. For example, the buffer flow velocity should be limited to complete the formation of pH gradient during the sample residence time,[2] and it should be small enough to complete the separation before the sample leaves the device. While it is possible to determine those design parameters through experimental trials and error, one better way to address this is through a robust and accurate model. Also model can address many surprising findings such as curious pH distributions in the

experimental work of open-flow isoelectric focusing in microchips.[9,10] In this study, a model is developed for FFIEF to investigate the effects of electric field and channel geometry for continuous and high resolution separation of proteins.

The rest of the paper is organized as follows. First, we present our mathematical model for mass, momentum, and charge conservation equations. Next, we present methods to calculate the net charge and mean square charge for proteins and ampholytes. We also describe a simplified method to calculate concentrations of hydrogen and hydroxyl ions using the electroneutrality condition. This is followed by our numerical methods to solve the coupled systems of partial differential equations for flow velocity, electric potential, and concentrations of components. Then we validate our numerical results by comparing with existing experimental work. Numerical results of FFIEF in a microfluidic device are presented considering the effect of cross-stream velocity in the system, and a novel design is proposed for enhancement of resolution. Finally, we provide our conclusions and recommendations for future works.

II. THEORY

A. Mathematical model of FFIEF

Understanding of FFIEF requires the knowledge of flow and electric fields as well as the pH field in the system. Due to the low Reynolds number creeping flow ($\mathrm{Re} \ll 1$), the flow field in a microfluidic device can be modeled with the momentum conservation (Stokes) equations along with the continuity equation as[11]

$$-\nabla p + \mu \nabla^2 \vec{V} + \rho_E \vec{E} = 0, \tag{1}$$

$$\nabla \cdot \vec{V} = 0, \tag{2}$$

where μ, $\vec{V}$, and p are the dynamic viscosity, bulk flow velocity, and hydrostatic pressure, respectively. The last term in Eq. (1) accounts for the electrokinetic body force due to electric charge density, ρ_E and the applied electric field, $\vec{E}$. The electric field is defined as

$$\vec{E} = -\nabla \phi, \tag{3}$$

where ϕ is the electric potential. The charge density can be obtained from the concentration of individual ionic component as

$$\rho_E = F \sum z_i C_i, \tag{4}$$

where F is the Faraday constant, z_i and C_i are the charge and concentration of each ionic component. For isoelectric focusing, these ionic components include amphoteric molecules such as proteins and ampholytes as well as hydronium and hydroxyl ions.

For dilute solution, the mass conservation equation for each ionic component can be calculated as[12]

$$\frac{\partial C_i}{\partial t} + \nabla \cdot \vec{N}_i = 0, \tag{5}$$

where $\vec{N}_i$ is the total flux which consists of flux due to electro-migration ($\vec{N}_{elec}$), diffusion ($\vec{N}_{diff}$), and bulk fluid motion ($\vec{N}_{bulk}$). The electro-migration velocity of charged analytes can be found from the electrophoretic mobility (ω), net charge ($\langle z \rangle$), and the applied electric field; the flux due to electro-migration velocity can be calculated as

$$\vec{N}_{elec} = -\langle z_i \rangle \omega_i \nabla \phi \, C_i. \tag{6}$$

The net charge value of a component i is due to the charge contributions of individual species discussed later.

From the Fick's law, the flux due to diffusion (D_i) can be formulated as

$$\vec{N}_{diff} = -D_i \nabla C_i, \tag{7}$$

and the mass flux of each component due to bulk flow velocity ($\vec{V}$) is

$$\vec{N}_{bulk} = \vec{V} C_i. \tag{8}$$

Finally, the mass conservation equation for each component can be rewritten based on Eqs. (5)–(8) as

$$\frac{\partial C_i}{\partial t} + \nabla \cdot \left(\vec{V} C_i - \langle z_i \rangle \omega_i \nabla \phi \, C_i - D_i \nabla C_i \right) = 0. \tag{9}$$

This equation is also known as the Nernst-Planck equation. The electric potential (ϕ) in the mass conservation equation is calculated from the following charge conservation equation:[13]

$$\frac{D\rho_E}{Dt} + \nabla \cdot \vec{i} = 0, \tag{10}$$

where $\vec{i}$ is the current density vector in the system. The current density is due to the movement of ionic component in the system under the action of applied electric field. For an electrolyte system, the current density can be expressed as

$$\vec{i} = \sum_{i=1}^{M} \left[F \vec{V}_{tot} (\langle z_i \rangle C_i) \right], \tag{11}$$

where M is the total number of components including hydrogen and hydroxyl ions. In Eq. (11), the total velocity of the buffer solution ($\vec{V}_{tot}$) consists of electro-migration velocity ($\vec{V}_{elec}$), diffusion velocity ($\vec{V}_{diff}$), and the bulk movement of buffer solution ($\vec{V}$). Thus, the governing equations for electric potential can obtained as

$$\nabla \cdot \left\{ -F \left[\sum_{i=1}^{M} \left(\langle z_i \rangle^2 \omega_i C_i \right) \right] \nabla \phi - F \left[\sum_{i=1}^{M} \left(\langle z_i \rangle D_i \nabla C_i \right) \right] + F \vec{V} \left[\sum_{i=1}^{M} \left(\langle z_i \rangle C_i \right) \right] \right\} = 0. \tag{12}$$

The boundary conditions for the mathematical model are presented in Table I.

B. Ampholyte and protein net charge

To solve the Nernst-Planck (Eq. (9)) and charge conservation (Eq. (12)) equations, one has to find the net charge of a component $\langle z_i \rangle$ and the mean square charge $\langle z_i^2 \rangle$. The detail description for this calculation is presented in our earlier work,[14] and in this study we briefly present them for self-sufficiency and clarity. If we consider each component i consists of j species, then the relationship between the concentration of species and components can be given as

TABLE I. Boundary conditions for the mathematical model. Here $\vec{n}$ is the surface unit normal.

	Mass conservation	Momentum conservation	Charge conservation
Inlet	C_i = Constant	Uniform inlet velocity	$\vec{n} \cdot \nabla \phi = 0$
Outlet	$\vec{n} \cdot \nabla C_i = 0$	Fully developed	$\vec{n} \cdot \nabla \phi = 0$
Left (side) wall	$\vec{N}_i = 0$	No slip and no penetration	ϕ = Constant
Right (side) wall	$\vec{N}_i = 0$	No slip and no penetration	ϕ = Constant

$$C_i = \sum_{j=0}^{J} S_{ij}, \tag{13}$$

and the net charge can be found from the species concentration (S_{ij}) and charge (z_{ij})

$$\langle z_i \rangle = \frac{\sum_{j=0}^{J} z_{ij} S_{ij}}{C_i}. \tag{14}$$

Similarly, the mean square charge of a component can be defined as

$$\langle z_i^2 \rangle = \frac{\sum_{j=0}^{J} z_{ij}^2 S_{ij}}{C_i}. \tag{15}$$

Here, it is assumed that component i has $J+1$ charge states, and the transition between adjacent states takes place by losing or gaining a proton. Thus, the charge of a species can be obtained as

$$z_{ij} = z_{i0} - j, \tag{16}$$

where z_{i0} is the most positive charge. For the aforementioned transition of states, the basic "mass-action" relationship between charge-adjacent species of the same component can be given as

$$S_{ij} + H_2 0 \leftrightarrow S_{ij-1} + H_3 0^+. \tag{17}$$

If the dissociation reactions are fast, the concentration of adjacent states are related as

$$S_{ij} = \frac{C_{H_3 0^+} S_{ij-1}}{K_{ij}}, \tag{18}$$

where K_{ij} are the equilibrium constants.

By substituting Eqs. (16) and (18) into Eq. (14), one can get

$$\langle z_i \rangle = z_{i0} - \tilde{z}_i, \tag{19}$$

where the number of protons removed from a molecule ($\tilde{z}_i$) can be given as

$$\tilde{z}_i = \sum_{j=1}^{J} \left[j \left(\frac{\prod_{k=1}^{j} K_{ik}}{(C_{H_3O^+})^j} \right) \right] \Bigg/ \left[1 + \sum_{j=1}^{J} \left(\frac{\prod_{k=1}^{j} K_{ik}}{(C_{H_3O^+})^j} \right) \right]. \tag{20}$$

Also, by substituting Eqs. (16) and (18) in Eq. (15), we have

$$\langle z_i^2 \rangle = (z_{i0})^2 - 2(z_{i0} - \tilde{z}_i) \cdot \tilde{z}_i + \tilde{z}_i^2, \tag{21}$$

where

$$\tilde{z}_i^2 = \sum_{j=1}^{J} \left[j^2 \left(\frac{\prod_{k=1}^{j} K_{ik}}{(C_{H_3O^+})^j} \right) \right] \Bigg/ \left[1 + \sum_{j=1}^{J} \left(\frac{\prod_{k=1}^{j} K_{ik}}{(C_{H_3O^+})^j} \right) \right]. \tag{22}$$

The aforementioned methods for finding the net charge and mean square charge are applicable for low molecular weight ampholytic components, such as the carrier ampholytes, for which the equilibrium constants (K_s) are known. However, for most proteins, the reaction rate constants are not readily available. Rather titration curve can be constructed easily for most proteins. Once a titration curve is known from the structure of the protein, the net charge is an explicit function of pH

$$\langle z_i \rangle = g_i(pH). \tag{23}$$

Thus, from the knowledge of pH at a location, the net charge of a protein can be obtained. The method of finding the mean square charge is more intricate. Mosher *et al.*[15] presented a technique to find the mean square charge of a protein from a titration curve as

$$\langle z_i^2 \rangle = [\langle z_i \rangle]^2 - \frac{1}{\ln 10} \frac{d\langle z_i \rangle}{dpH}. \tag{24}$$

C. Simplified mathematical model for FFIEF

In FFIEF, the concentration of other ionic components such as hydrogen (H) and hydroxyl (OH) ions can also be described by Nernst-Planck equation. In that case, one has to solve M partial differential equations for the concentration of each component in the system in addition to the charge conservation equation for the electric field. Though the numerical scheme needed for solving the concentrations of hydrogen and hydronium ions is similar to any other mass conservation (Nernst-Planck) equations, the convergence of solutions is very challenging for hydrogen and hydronium ions because of 4–6 orders difference in magnitude in their concentration value. Thus, to circumvent the numerical stiffness, one can use the electroneutrality condition to find the concentration of hydrogen ion (C_H) as

$$\sum_{i=1}^{M-2} (\langle z_i \rangle D_i \nabla C_i) + C_H - \frac{K_W}{C_H} = 0, \tag{25}$$

where K_w is the equilibrium constant for water. Here, the first term considers the contributions of all amphoteric molecules (both proteins and ampholytes), while the second and third terms are due to hydrogen and hydronium ions, respectively. From electroneutrality, the last term of charge conservation equation (Eq. (12)) is also dropped out, and the modified charge conservation equation can be rewritten as

$$\nabla \cdot \left\{ -\lambda \nabla \phi - F \left[\sum_{i=1}^{N} (\langle z_i \rangle D_i \nabla C_i) + D_H \nabla C_H - D_{OH} \nabla \frac{K_W}{C_H} \right] \right\} = 0. \tag{26}$$

Here, ionic conductivity (λ) is defined as

$$\lambda = F \left[\sum_{i=1}^{N} \langle z_i \rangle^2 \omega_i C_i + \omega_H C_H + \omega_{OH} \frac{K_W}{C_H} \right]. \tag{27}$$

It is noteworthy to mention that the electroneutrality condition is not valid close to the wall where the electric double layer might form. Thus, for nanochannel free flow IEF, one has to solve the Poisson-Nernst-Planck model.[16,17] However, in this study, the length scale of the electric double layer is 3–4 orders of magnitude smaller than the length scale of typical microfluidic device used for FFIEF. Moreover, IEF channels are generally coated with chemicals to eliminate the electric double layer formation.[18,19] Using electroneutrality equation, the momentum conservation equation can be rewritten as

$$-\nabla p + \mu \nabla^2 \vec{V} = 0. \tag{28}$$

Thus, the complete mathematical description for FFIEF consists of Eqs. (2) and (28) for fluid flow; Eqs. (9) and (25) for concentration of amphoteric components and hydrogen ions; and Eq. (26) for electric potential.

D. Numerical scheme

The numerical algorithm used to calculate the flow velocity, concentration of amphoteric component, and electric potential is shown in Figure 2. In this study, the discretized algebraic equations are derived for mass, momentum, and charge conservation equations using finite volume method.[20,21] The power law scheme is used to compute the flux terms in all equations. The unsteady term in Nernst-Planck equation is modeled with a first order accurate implicit scheme. For the fluid flow equations, the co-located semi-implicit method for pressure linked equations (cSIMPLE) algorithm[22] is used to find the pressure and velocity fields through an iterative scheme. In this work, the system of linear algebraic equations is solved using line by line Thomas algorithm[23,24] owing to the tri-diagonal matrix system. The convergence tolerances are 10^{-4} for continuity and momentum equations and 10^{-5} for mass and charge conservation equations. To reduce the computational time, we have developed a parallel algorithm[14] using OpenMP.[25] Numerical simulations are performed on an Intel Xeon 2.3 GHz (16 threads) and each simulation result is obtained in 5 days.

III. RESULTS AND DISCUSSION

A. Model verification

To verify the FFIEF model, we compare our numerical results with the experimental findings of Kohlheyer *et al.*,[5] where they have presented the concept of free flow IEF in a straight

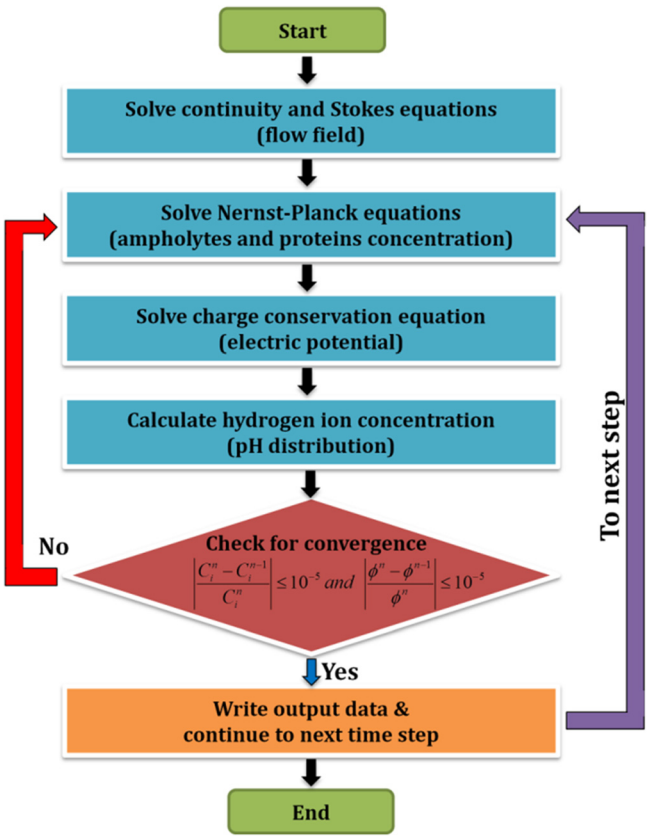

FIG. 2. The numerical algorithm for simulation of FFIEF. Here, C_i^n and ϕ^n are the concentration of each component i and electric potential at nth iteration step.

microchannel. Unlike the experimental work of Cabrera and Yauger,[4] a sheath flow of H_2SO_4 and NaOH was introduced in the anodic and cathodic sides to avoid the bubble formation. These sheath flows eliminated the bubble formation problem in IEF, but it did not affect the sample separation phenomena. Stable pH gradient formation was demonstrated in their microchannel using an applied electric field of 200 V/cm. Figure 3(a) (symbols) shows an almost linear pH profile at the end of their microchannel, where the pH values were obtained from the locations of 7 p*I* markers used in their experimental study.[5,6]

To validate our model, we have simulated an identical case considering the 7 p*I* markers used in the experimental work of Kohlheyer *et al.*[5] The physico-chemical properties of p*I* markers are listed in Table II. The pH gradient is created using 48 biprotic ($\Delta pK = 2.5$) ampholytes[24] having isoelectric points between pH of 3.7 and 10.3. In other words, 48 mass conservation equations are solved to create the pH distribution for isoelectric focusing of proteins. It is important to note that an increase in the number of ampholytes will make a smoother pH profile for IEF. But we kept the number of ampholytes below 50 to keep the computational expenses reasonable for multidimensional IEF.

The numerical simulation is only carried out in the effective separation chamber (5 mm $\times$ 0.8 mm $\times$ 10 μm), where there is no influence of the sheath flow. Thus, there is no need to consider the effect of acid and base in the numerical model simplifying the calculation. The pH

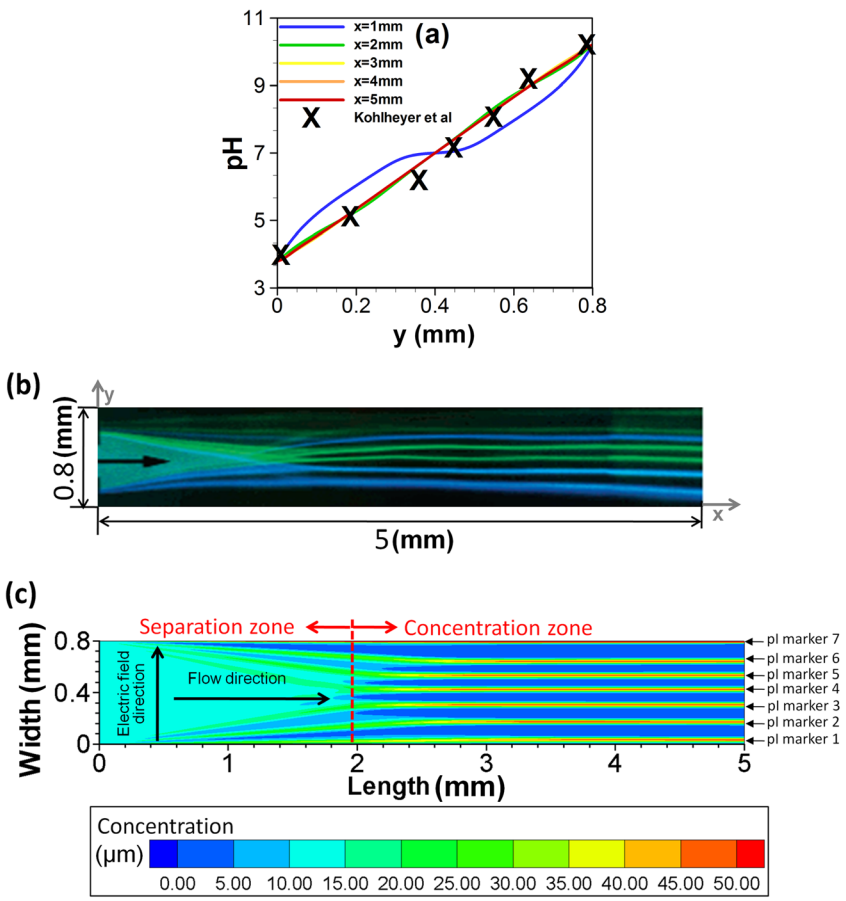

FIG. 3. (a) pH distributions across the channel at the channel outlet. Here symbols are from the experimental data of Kohlheyer *et al.*[5] for a FFIEF channel, while the solid lines are from the numerical results of an identical system. The concentration contours of p*I* markers from (b) experimental work (Reproduced with permission from Kohlheyer *et al.*, Anal. Chem. **79**, 8190 (2007). Copyright 2007 American Chemical Society) and (c) numerical simulation work. The p*I* makers, which are uniformly introduced at channel inlet, are concentrated at their isoelectric points and fully separated at the channel outlet. Depending on the pattern of separation, FFIEF column can be divided into separation and concentration zones. The applied (nominal) electric field is 200 V/cm and the mean flow velocity is 1 mm/s.

TABLE II. Physico-chemical parameters for p*I* markers used in Ref. 5.

	pK_1	pK_2	pI	ω [m^2/Vs]
pI marker 1	3.20	4.80	4.00	3.0×10^{-8}
pI marker 2	3.94	6.30	5.12	3.0×10^{-8}
pI marker 3	5.35	6.95	6.15	3.0×10^{-8}
pI marker 4	6.20	8.10	7.15	3.0×10^{-8}
pI marker 5	6.80	9.30	8.05	3.0×10^{-8}
pI marker 6	8.05	9.85	8.95	3.0×10^{-8}
pI marker 7	9.95	10.65	10.30	3.0×10^{-8}

distributions obtained from the numerical results are presented on Figure 3(a) as solid lines. The numerical results show that the pH profile is not linear near the entry (x = 1 mm) region, but a linear pH profile can be formed as the buffer solution flows downstream. Our numerical results indicate that a stable and linear pH profile can be achieved within the 2 mm of the channel entry for a flow velocity of 1 mm/s. The numerical results agree well with the experimental observations verifying the model developed here.

We also qualitatively validate the location of p*I* markers used in the experimental work of Kohlheyer *et al*.[5] Figure 3(b) shows the locale of experimental p*I* markers in the channel, while the Figure 3(c) shows our numerical predictions with the same conditions. The contour plots show similar trends in both experimental and numerical works of FFIEF. It is important to note that a uniform mixture of p*I* markers is introduced at the entry region of the channel along with a soup of carrier ampholytes. The p*I* markers are separated as the buffers moved downstream with flow and each maker is totally separated at or near the isoelectric point at the end of channel (see Figure 3(c)). Based on the separation pattern, the FFIEF channel can be classified into the separation zone and concentration zone. In the separation zone, lateral position of isoelectric point is changing as samples are flowing downstream. On the other hand, in the concentration zone, samples are concentrated at their isoelectric points without any further change in their lateral positions (see Figures 3(b) and 3(c)).

B. Protein separation in a straight microchannel

In this section, we present the protein separation capability of FFIEF in a straight microchannel. The numerical simulations of FFIEF are carried out in a 6 mm (long) × 3 mm (wide) channel considering two proteins: cardiac troponin I and serum albumin. The pH gradient in the channel is formed using 48 carrier ampholytes ($\Delta pK = 2.5$), and the isoelectric points of these ampholytes are within the pH range of 5–8. Transport properties of carrier ampholytes, proteins, and other ionic components are listed in Table III. The net charge values of serum albumin and cardiac troponin I (cTnI) are obtained from the protein data bank[26,27] for different pH, and the titration curves are constructed using the Fourier series which are presented in

TABLE III. Physico-chemical parameters for ampholytes, proteins, hydrogen ions, and hydroxyl ions.

Buffer solution dynamic viscosity		μ	1.002 [mPa-s]
Electrophoretic mobility	Ampholyte	ω_{amp}	3×10^{-8}[m^2/V-s]
	cTnI	ω_{cTnI}	1.56×10^{-8}[m^2/V-s][29]
	Albumin	ω_{ALB}	2.0×10^{-8}[m^2/V-s][29]
	Hydrogen ion	ω_{H^+}	36.25×10^{-8}[m^2/V-s][30]
	Hydroxyl ion	ω_{OH^-}	20.50×10^{-8}[m^2/V-s][30]
Diffusivity of components		D_i	$\omega_i RT/F$[m^2/s]
Dissociation constant of proton ion in water solution		K_W	1.0×10^{-14} (molarity based)

Figure 4. These titration curves are used to find the mean square charge of proteins using Eq. (24).

The buffer solution of carrier ampholytes is first introduced in the separation channel at a flow velocity of 1 mm/s, and a potential difference of 80 V is applied between anodic and cathodic sides to form the pH gradient in the channel. Figures 5(a) and 5(b) show the pH profile in the separation channel at the end of the stabilization phase. Here, the stabilization phase is similar to steady state when the pH profile in the channel does not change with time. Near the channel entry, the pH profile is quite nonlinear as ampholytes are moving due to advection and trying to focus at their isoelectric points due to electromigration. But at the end of the channel, a nearly linear pH profile (see Figure 5(b)) is formed which is very conducive for separation of proteins.

At the end of the (ampholyte) stabilization phase, a uniform mixture of sample proteins is introduced to the separation channel continuously. This is very similar to the experimental work of Cheng and Chang[9] in which they introduced the sample mixture in the separation channel after forming the pH profile using an actuator. Figure 5(c) shows the protein concentration

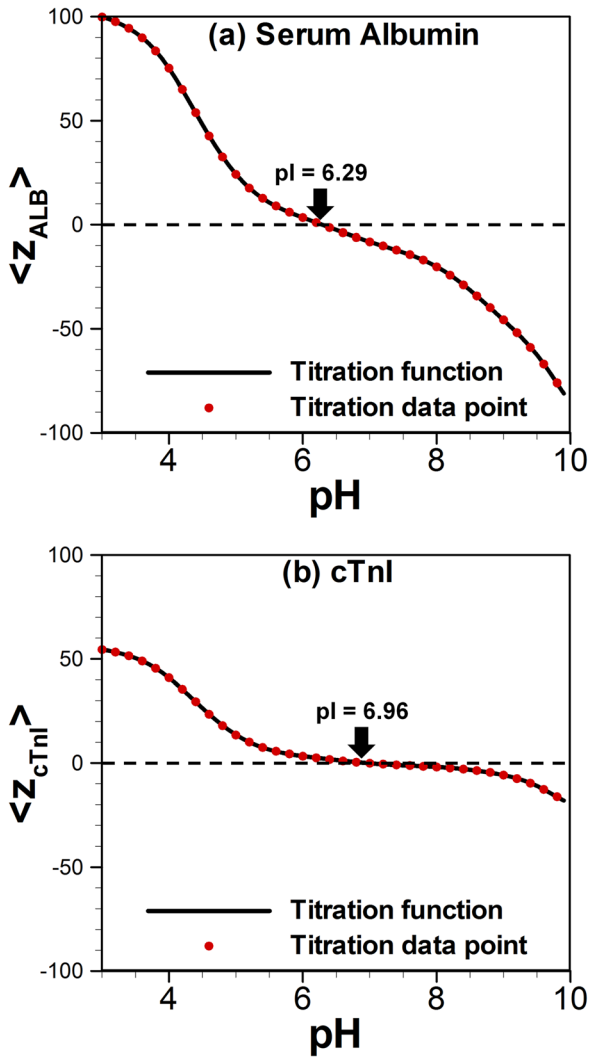

FIG. 4. Titration curves for (a) human serum albumin and (b) cTnI (adult cardiac troponin I). The p*I* points for serum albumin and cTnI are 6.29 and 6.96, respectively. The titration curves used in this study are formed from the protein sequence. First, the sequence of a particular protein is obtained from UniProt.[26] Next, the protein sequence is exported to a protein calculator[27] to obtain charge distribution at different pH values. In this study, a Fourier series is used to form the smooth titration curves from charge data. The titration curve is used subsequently to find net charges and mean square charges.

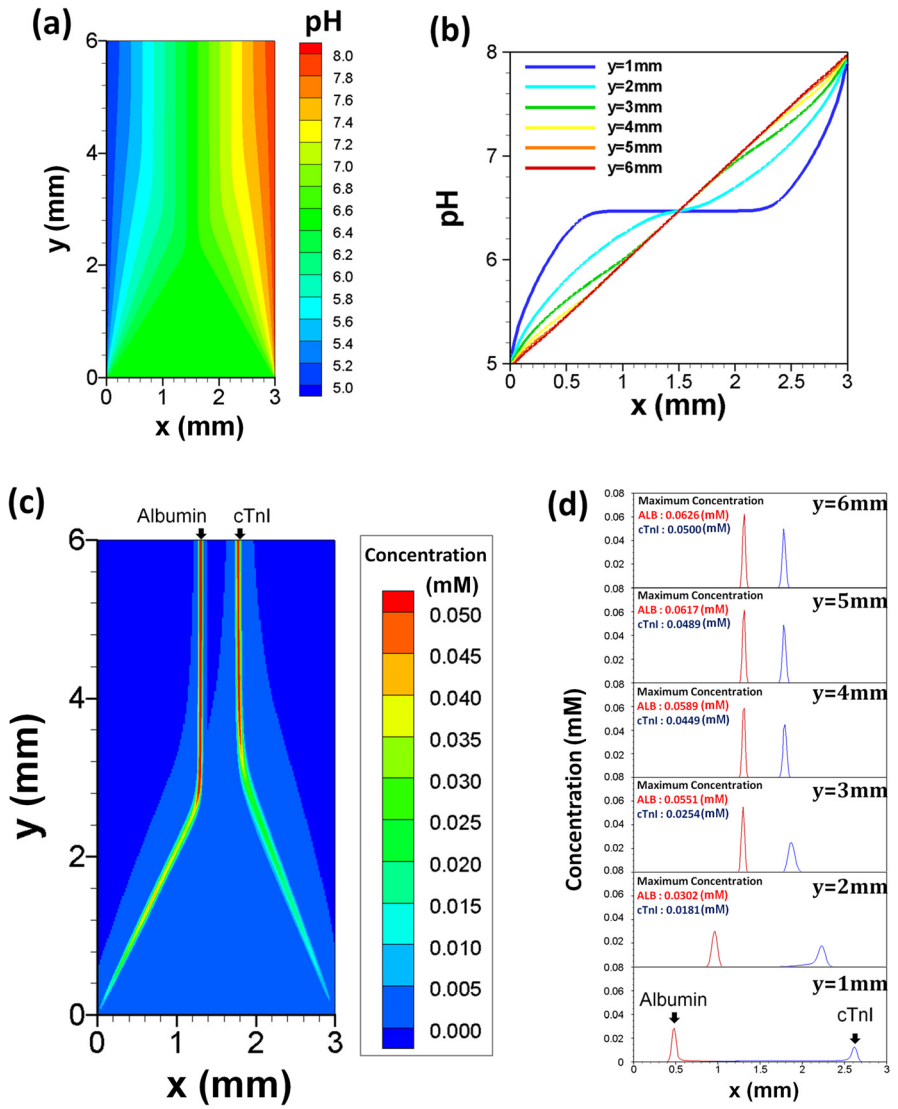

FIG. 5. Simulation results of FFIEF in a straight microchannel for a mean flow velocity of 1 mm/s and an applied electric potential difference of 80 V. (a) pH contour profile. (b) pH distributions across the channel at y = 1/2/3/4/5/6 mm. It takes 30 s to form a stable pH profile using 48 biprotic ampholytes, and a nearly linear pH profile is formed at the end of the channel. Concentration contour (c) and profiles (d) for albumin and cTnI in a straight microchannel at t = 60 s. Proteins are focused at their isoelectric points and the horizontal/lateral (x) locations of focused proteins don't change after y = 3 mm.

contours at the steady state, which is achieved within 60 s of the initiation of the separation process. Although simulation results are performed for unsteady FFIEF, only steady state results are presented because of its relevance to protein chip scenario where the samples are collected when steady state is reached. Similar to the pH profile, the concentration distributions are also position dependent and evolve as the sample moves downstream with fluid flow. Near the channel entry (see Figure 5(d)), albumin and cTnI peaks form at the left and right side of the channel, respectively. As these proteins move downstream, the focusing points start shifting towards inside in the cross-stream (x) direction. The focusing points stop moving in the cross-stream direction any further once they reach ~3 mm along the streamwise (y) direction. After that location, the peak concentrations of proteins continue to grow as they move towards the downstream direction. In other words, for y > 3 mm, the proteins are focused at their stationary isoelectric points for the case presented here. Thus, we can refer to any region before and after y = 3 mm as the separation (focusing) zone and concentration zone, respectively. At the end of

the channel, the concentrations of albumin and cTnI have increased 54 and 47 fold, respectively, from their initial values. Albumin forms tighter bands compared to cTnI because the slope of the titration curve is steeper for albumin compared to cTnI (see Figure 4). The simulation result also reveals that two proteins can be totally separated near the channel outlet.

To investigate the effect of the applied electric field in the protein separation phenomena, FFIEF simulations are carried out for different applied electric field scenarios. The applied electric potential difference between anode and cathode sides are varied between 40 V and 160 V, while keeping all other simulation conditions the same as discussed in Sec. III B. The concentration contours of albumin and cTnI proteins are shown in Figure 6 for nominal electric field of 133.3 V/cm and 533.3 V/cm. Simulation results indicate that the length of the focusing zone is shorter as the applied electric field is increased. For instance, the length of the focusing zone is 6 cm for a nominal electric field of 133.3 V/cm, while this value is 3 cm and 1.5 cm for nominal electric field of 266.7 V/cm and 533.3 V/cm, respectively. Moreover, the protein peak concentration highly depends on applied electric potential difference. In particular, for lower applied electric field (Figure 6(a)) proteins are still focusing near the channel outlet as evidenced by the changes in the peak concentration locations. Therefore, an adequate electric field should be applied to complete the focusing within the channel length. Higher applied electric field will ensure complete separation of proteins in addition to providing tightly focused protein bands. However, a higher electric field will result in significant Joule heating in the system which may adversely affect the protein separation performance.[28]

C. A new channel design for high resolution FFIEF separation

In protein separation work, the performance of a separation process is estimated by the resolution. The separation resolution (R_{ij}) between two proteins (i and j) can be estimated as

$$R_{ij} = \frac{|x_{f,i} - x_{f,j}|}{2\sigma_i + 2\sigma_j}, \tag{29}$$

where x_f and σ are the location of concentration peak and the standard deviation of concentration band, respectively. Equation (29) indicates that the tightly focused protein bands and/or a large separation distance between peak points can ensure high resolution. As shown earlier, the tightly formed protein bands can be formed using higher electric field. However, there is an upper limit on applied electric field strength since the proteins might be denatured at high

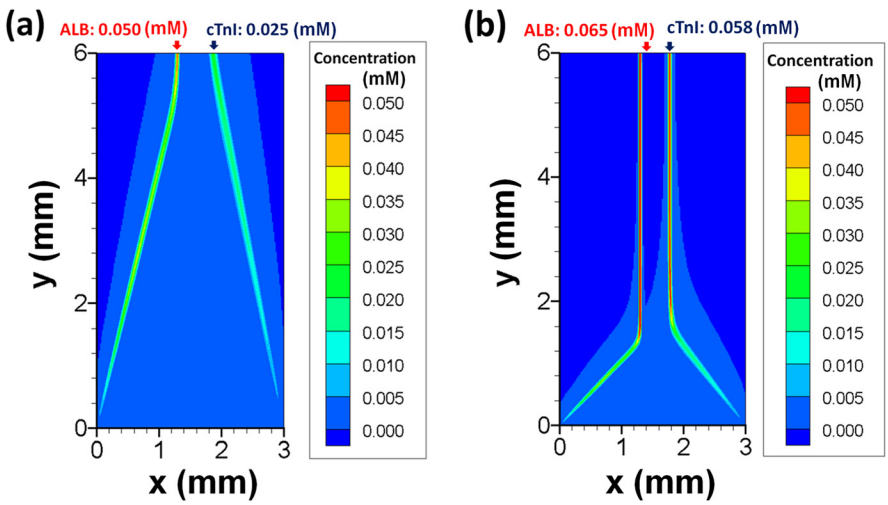

FIG. 6. Effect of applied electric field in the pH formation. Protein concentration contours for an applied electric potential difference of (a) 40 V and (b) 160 V. All other simulation conditions are the same as in Figure 5. The length of focusing zone is reduced as applied electric potential difference is increased.

temperature due to Joule heating. An alternative approach to improve the resolution is to increase the distance between the focused protein peaks. In a straight channel, the focused (isoelectric) point for a protein is primarily determined by the pH profile formed by the carrier ampholytes, and a laminar flow cannot change the p*I* locations appreciably. In a straight channel, the streamwise flow (not shown) becomes parabolic (in the z-direction) at the end of the separation channel, and there is no noticeable cross-stream flow velocity (Figure 7(b)) for any influence on the change in the location of p*I* points. However, the flow velocity can be perturbed by introducing a channel insert/post at the end of the separation channel. Figures 7(c) and 7(d) show the streamwise and cross-stream velocity distributions along a microchannel when a post/block is placed at the end of the channel between x = 1 mm and x = 2 mm. This post blocks 1/3 of the flow area compared with the case shown in Figures 7(a) and 7(b) where the channel is fully open. Moreover, this post creates significant cross-stream velocity, which can be exploited to increase the focusing distance between the two adjacent protein bands.

Figure 8 shows the effect of cross-stream flow on the sample separation and concentration in FFIEF channel where a flow block is inserted at the channel exit. The behavior of pH formation and protein separation is similar to fully open channel (Figure 5) until y = 4 mm. Beyond that point the effect of cross-stream flow becomes important and it makes a significant change in the isoelectric focusing process. Figure 8(b) shows that the pH profile becomes flat at the end of the separation channel when a block is introduced at the end of the channel. This flat pH profile increases the physical distance between two p*I* points, which essentially increase the distance between two protein bands (Figure 8(d)). Unlike the fully open channel case presented

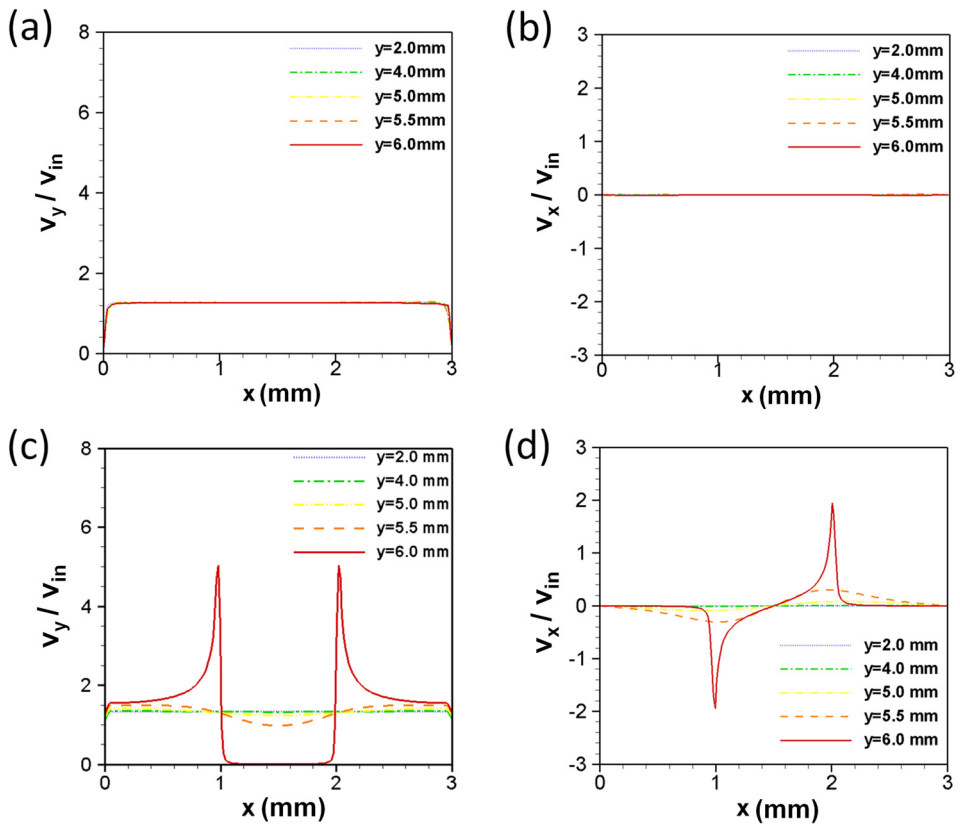

FIG. 7. Flow velocity distribution in FFIEF channels. Streamwise (a) and cross-stream (b) velocity for a separation channel (6 mm × 3 mm × 10 μm) used for Figures 5 and 6. There is no noticeable cross-stream velocity at the downstream of a straight microchannel due to fully developed low Reynolds number creeping flow. Streamwise (c) and cross-stream (d) velocity for a higher resolution separation channel (6 mm × 3 mm × 10 μm). Cross-stream velocities are created by partially blocking the channel exit between x = 1 mm and x = 2 mm. These cross-stream velocities are exploited to increase the separation resolution by increasing the separation distance between focused peaks.

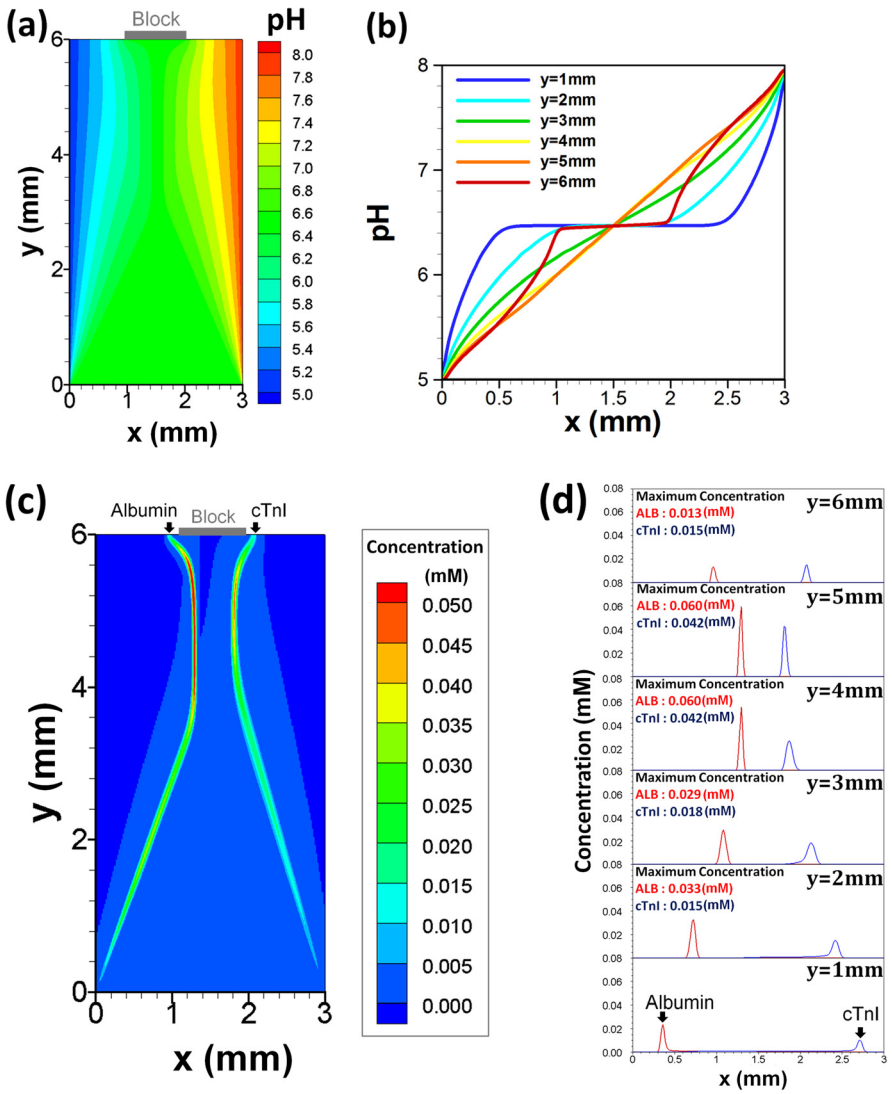

FIG. 8. Simulation results of FFIEF in a high resolution separation channel for a mean flow velocity of 1 mm/s and an applied electric potential difference of 80 V. (a) pH contour profile. (b) pH distribution across the channel at y = 1/2/3/4/5/6 mm. It takes 60 s to form a stable pH profile using 48 biprotic ampholytes, and a nearly flat pH profile is formed at the mid section of the channel exit due to flow blockage. Concentration contour (c) and profiles (d) for albumin and cTnI at t = 120 s.

in Figure 5(d), the separation distance between the two proteins decreases during the focusing phase, while it increases during the concentration phase. Although the cross-stream flow increases the distance between the focused proteins, it reduces the concentration of protein peak. However, the effect of reduction in peak height is much less compared with the increase in separation distance. To quantify the relative merits and pitfalls of the new design, the separation resolution is presented in Figure 9 for both fully open channel (case A) and the channel partly blocked at the exit (case B). For the fully open case, the resolution increases until y = 4 mm due to the focusing of proteins at their p*I* points, while decreases slightly afterwards due to decrease in the focusing distance while maintaining the peak width and height. On the other hand, for case B, the resolution decreases first due to the decrease in separation distance, but increases after y = 4 mm due to the increase in separation distance due to cross-flow. Figure 9 shows that the resolution increases three folds once the cross-stream velocity is introduced using a post/block at the channel exit. This simple design is very helpful to increase the separation distance while maintaining relatively low electric field strength.

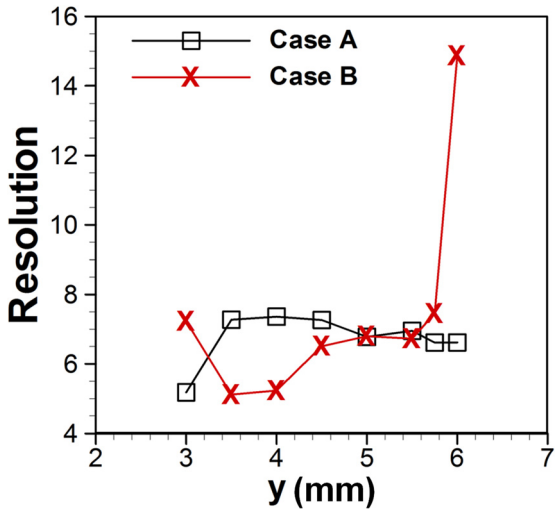

FIG. 9. FFIEF separation performance for fully open separation channel (case A) and partially blocked separation channel (case B).

Although the channel design presented in case B uses the identical isoelectric focusing conditions (number of ampholytes, applied electric field, etc.) as in case A, the fluid flow condition is quite different in case B. The flow blockage caused by the post results in a higher pressure drop in case B compare to case A as shown in Figure 10. Therefore, one has to use high pumping power to operate case B configuration. More importantly, it takes longer time to obtain the focusing and separation. For instance, the stabilization and separation times are 30 s and 60 s for fully open channel case A, while it takes 60 s to form stable pH profile and 2 min for complete separation of cTnI and albumin in case B. Nevertheless, the insertion of a post at the channel exit can be exploited to increase the separation resolution. This is especially useful for separation of proteins having much closer p*I* points. However, in this case the position of the post has to be adjusted based on the pI points of proteins. Figure 11 shows the concentration distribution of two proteins (Hemoglobin subunit B (HBB) and G (HBG)) in a microchannel for a nominal applied electric field of 266.7 V/cm and an inlet flow velocity of 1 mm/s. In this case, the final focused points of both proteins are located at the right half of the channel when no post is used (Figure 11 (left)). However, the final separation distance as well as the

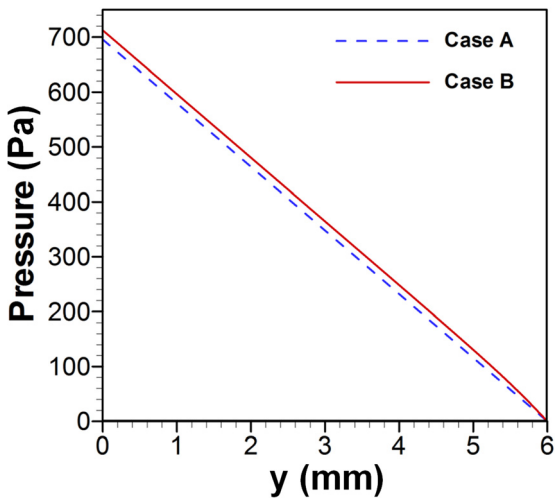

FIG. 10. Pressure distribution along the separation channel for fully open and partially blocked outlet. The maximum pressure drops for fully open and partially blocked outlet are 695 Pa and 712 Pa, respectively.

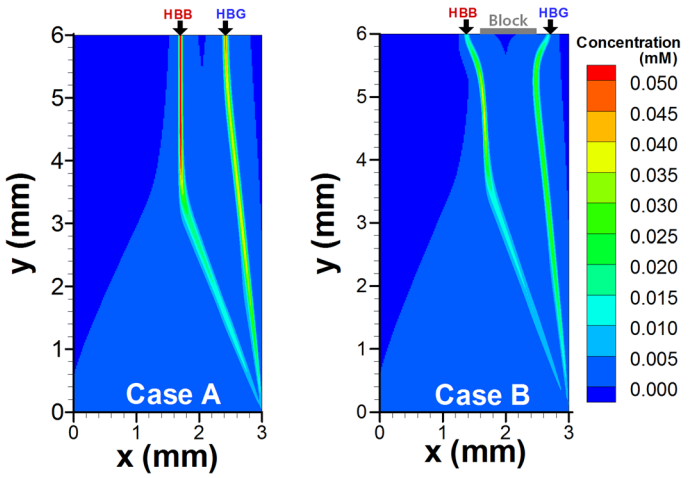

FIG. 11. Simulation results of FFIEF for fully open (case A) and partially blocked (case B) channel. The numerical simulations of FFIEF are carried out in a 6 cm (long) × 3 cm (wide) channel considering two proteins: Hemoglobin (subunit) B (HBB) and G (HBG). The isoelectric points of HBB and HBG are 7.27 and 8.21, respectively. The pH gradient in the channel is formed using 48 carrier ampholytes having ΔpK of 2.5, and the isoelectric points of these ampholytes are within the pH range of 5–9. The inlet flow velocity is 1 mm/s. A nominal electric field of 266.7 V/cm is applied to form the pH gradient in the channel. Here, the pressure drop between inlet and outlet are 695 Pa and 716 Pa for case A and case B, respectively. The separation resolution is 7.9 and 11.7 for fully open (case A) and for partially blocked (case B), respectively.

separation resolution can be improved significantly by placing a block between x = 1.5 mm and x = 2.6 mm (Figure 11 (right)). The separation resolution of proteins having very close isoelectric points can be improved by reducing the width of the separation post (not shown) as well as by using narrow pH range for ampholytes.

IV. SUMMARY AND CONCLUSIONS

A mathematical model is developed to simulate the FFIEF considering the mass, momentum, and charge conservation equations. The governing partial differential equations are solved using the co-located finite volume method. To obtain numerical simulation results in a reasonable time, an in house numerical code is developed using OpenMP based parallel scheme. Numerical results obtained from this model are compared with the existing experimental work; an excellent agreement is obtained between numerical and experimental work where pH profile development and separation of p*I* markers are considered. Numerical simulations are carried out for FFIEF considering 48 ampholytes and 2 real proteins for an applied electric field range of 133 V/cm to 533 V/cm. The electric field is introduced to focus carrier ampholytes and proteins at their isoelectric points. The focused ampholytes first formed the required pH profile in the system for the separation of proteins from an initial uniform mix, while the flow field is applied to collect the separated proteins. The numerical results reveal that the pH profile is formed as buffer solution goes downstream and analytes can be totally separated at the channel outlet.

The effects of electric and flow fields are particularly considered in this study. The flow field effect is introduced by changing the channel design. Two different channel designs are considered in this study. The first design is based on a straight microchannel, while, in the second design, a post is inserted at the end of a straight microchannel to disturb the flow. The fully open outlet channel in the first design produces parabolic streamwise velocity, but no cross-stream velocity at the end of the channel. On the other hand, the partially blocked outlet in the second design creates significant cross-flow which improves the separation resolution by increasing the separation distance between the focused peaks. Even though no changes in the electrochemical condition are needed in the second design to achieve higher resolution, the pumping pressure drop is little higher in the second design. Moreover, it takes longer time in the second design for formation of stable pH profile as well as separation of proteins. The

applied electric field strength has direct effect on higher separation resolution and shorter channel length. However, higher electric field might cause dispersion in separated proteins as well as denaturation of proteins due to elevated temperature.

ACKNOWLEDGMENTS

This work was supported in part by the US National Science Foundation under Grant No. CBET 1250107.

[1]K. Hannig, Fresenius' J. Anal. Chem. **181**, 244 (1961).
[2]H. Wagner, Nature **341**, 669 (1989).
[3]L. Krivankova and P. Bocek, Electrophoresis **19**, 1064 (1998).
[4]C. R. Cabrera and P. Yager, Electrophoresis **22**, 355 (2001).
[5]D. Kohlheyer, J. C. T. Eijkel, S. Schlautmann, A. van den Berg, and R. B. M. Schasfoort, Anal. Chem. **79**, 8190 (2007).
[6]D. Kohlheyer, J. C. T. Eijkel, S. Schlautmann, A. van den Berg, and R. B. M. Schasfoort, Anal. Chem. **80**, 4111 (2008).
[7]J. Wen, J. W. Albrecht, and K. F. Jensen, Electrophoresis **31**, 1606 (2010).
[8]J. Wen, E. W. Wilker, M. B. Yaffe, and K. F. Jensen, Anal. Chem. **82**, 1253 (2010).
[9]L. J. Cheng and H. C. Chang, Lab Chip **14**, 979 (2014).
[10]L. J. Cheng and H. C. Chang, Biomicrofluidics **5**, 046502 (2011).
[11]M. W. Frank and F. M. White, *Fluid Mechanics* (McGraw-Hill, New York, New York, 1979).
[12]J. S. Newman, *Electrochemical Systems* (Prentice-Hall, Englewood Cliffs, NJ, 1972).
[13]A. P. S. Bhalla, R. Bale, B. E. Griffith, and N. A. Patankar, J. Comput. Phys. **256**, 88 (2014).
[14]K. Yoo, J. Shim, J. Liu, and P. Dutta, Electrophoresis **35**, 638 (2014).
[15]R. A. Mosher, D. A. Saville, and W. Thormann, *The Dynamics of Electrophoresis* (VCH, Weinheim; New York, 1992).
[16]M. Pribyl, D. Snita, and M. Marek, Chem. Eng. J. **105**, 99 (2005).
[17]J. Lindner, D. Snita, and M. Marek, Phys. Chem. Chem. Phys. **4**, 1348 (2002).
[18]H. C. Cui, K. Horiuchi, P. Dutta, and C. F. Ivory, Anal. Chem. **77**, 1303 (2005).
[19]H. C. Cui, K. Horiuchi, P. Dutta, and C. F. Ivory, Anal. Chem. **77**, 7878 (2005).
[20]J. Shim, P. Dutta, and C. F. Ivory, Electrophoresis **28**, 572 (2007).
[21]J. Shim, P. Dutta, and C. F. Ivory, Numer. Heat Trans. **52**, 441 (2007).
[22]T.-K. J. Sze, J. Liu, and P. Dutta, J. Fluids Eng. **136**, 021206 (2013).
[23]J. Shim, P. Dutta, and C. F. Ivory, Electrophoresis **29**, 1026 (2008).
[24]J. Shim, P. Dutta, and C. F. Ivory, J. Nanosci. Nanotechnol. **8**, 3719 (2008).
[25]R. Chandra, *Parallel Programming in OpenMP* (Morgan Kaufmann Publishers, San Francisco, CA, 2001).
[26]See http://www.uniprot.org for UniProt, March 3, 2009 edition.
[27]C. Putnam, 3.3 ed., http://www.scripps.edu/~cdputnam, 2006.
[28]A. S. Rathore, J. Chromatogr. A **1037**, 431 (2004).
[29]D. Bottenus, M. R. Hossan, Y. Ouyang, W.-J. Dong, P. Dutta, and C. F. Ivory, Lab Chip **11**, 3793 (2011).
[30]A. B. Duso and D. D. Y. Chen, Anal. Chem. **74**, 2938 (2002).